A COMPOSITE ANISOGRID PANEL WITH SKIN: MECHANICAL TESTING AND DIC

G. Totaro[1], C. Ferrara[2] and F. De Nicola[3]

[1]CIRA – Italian Aerospace Research Center, Structures and Materials, 81043, Capua, Italy
g.totaro@cira.it, http://www.cira.it
[2]Sapienza University, Via Salaria, 00138, Rome, Italy
claudio_ferrara@live.it
[3]CIRA – Italian Aerospace Research Center, Structures and Materials, 81043, Capua, Italy
f.denicola@cira.it

Keywords: composite anisogrid panel, compression test, Digital Image Correlation.

Abstract

The axial compression test on a composite anisogrid panel with skin is discussed in the paper. The interpretation of the test results is enhanced via digital image correlation based on a stereo-camera system. The panel was extracted from the cylindrical prototype of the interstage structure realized by interlacing carbon fiber tows forming a regular system of hoop and helical ribs, and completed with an outer skin. A similar panel, without the skin, was previously extracted from the same prototype and tested under compression, demonstrating the occurrence of the lateral buckling mode of the ribs. Thus, the main objective of this work is to evaluate the effect of the skin on the strength of the anisogrid panel under axial compression. The stereo-camera system was set up on the skin side, in order to avoid the complexity of the anisogrid pattern. A fully 3D finite-element model of the panel was also constructed and analysed in order to simulate the test. The use of the stereo-camera system allowed us to highlight the onset of failures, and to better interpret the overall structural behaviour and the global stiffness of the panel.

1. Introduction

The axial compression test on a composite anisogrid panel with the outer skin is discussed in the paper. The interpretation of the test results is enhanced via digital image correlation (DIC) based on a stereo-camera system, namely, the VIC-3D™ System. The test-article (Fig. 1, on the left) is part of the prototype of the interstage structure presented in [1]. This prototype was realized by interlacing dry carbon fiber tows forming a regular system of hoop and helical ribs, completed with a dry outer skin. The overall dry preform was then co-infused under vacuum bag and co-cured out-of-autoclave.
A similar panel without the skin (see Fig. 1, on the right) was previously extracted from the same prototype and tested under compression, demonstrating the occurrence of a typical lateral buckling mode which reduces the load capability of the structure [2]. This lateral buckling mode is not necessarily limited to a panel, but can involve the overall structure as shown in [3]. We remark that composite anisogrid structures are normally designed without the skin, that is, the effect and the mass of the skin are neglected at the beginning of the design phase [4]. The hoop skin is usually thin and does not provide a primary structural role, which is instead provided by the system of ribs. Nevertheless, even a thin skin may exert a constraint on the ribs that is not considered in the preliminary design phase. Such constraint, indeed, turns out to be quite useless in view of global buckling failure modes and global stiffness properties of the structure. Conversely, the skin should be effective in correspondence of lateral buckling modes like the one previously verified.

Excerpt from ISBN 978-3-00-053387-7

Thus, the main objective of this work is to experimentally evaluate the effect of the skin on the strength of the anisogrid panel subject to a lateral buckling mode under axial compression. Similarly to the foregoing test, the panel is constrained between two metallic end flanges with a resin potting in correspondence of the upper and lower edges (hoop ribs). The panel is equipped with strain-gauges located in correspondence of helical ribs and with additional strain-gauges placed on the outer skin in the center of the panel, in order to obtain reference values for the stereo-camera acquisition. For this preliminary experience with the DIC technique, the stereo-camera system was installed on the skin side of the panel in order to avoid the complexity of the pattern of ribs. Moreover, a fully 3D finite-element (FE) model of the panel was also constructed and analysed in order to simulate the test. The use of the stereo-camera system allowed us to highlight the onset and the location of failures and to better interpret the overall structural behaviour of the panel. More details of this experimental work can be found in [5].

2. Axial compression test

The anisogrid test-articles with and without skin are shown in Fig. 1. According to [1], the panel without skin demonstrates a peculiar failure mode under axial compression which involves the lateral buckling of the system of ribs. The maximum load corresponding to this failure mode was about 100 kN. For the test under study, ten strain-gauges were located in correspondence of the central section of the panel with the following scheme: 7 on helical ribs, one on the hoop rib and two on the outer side of the skin in hoop and axial direction, respectively, in view of correlation with DIC measurements. The cross-head speed was set to 1.0 mm/min, the test ended in about 140 seconds. The plot in Fig. 2 shows a linear trend of the load-displacement curve, with two points of discontinuity due to local failures before the collapse. The first discontinuity occurs at about 111 kN, the second one at 147 kN, whereas the collapse occurs at 171 kN. Strain-gauge curves (Fig. 3) show a similar linear trend during the test, except for the two discontinuities already mentioned. In addition, it can be seen that, just before the collapse, strain-gauges curves N°1 and N°2 suddenly change their curvatures, remarking the onset of lateral deformation of corresponding ribs (i.e., local lateral buckling) at about 160 kN. In fact, rib N°1 (Fig. 4, on the right) bends with the convexity on the side of the strain-gauge (with a consequent strain reduction), whereas rib N°2 bends with the convexity on the opposite side of the strain-gauge (with a consequent increase of negative strain).
The panel after the mechanical test is visible in Fig. 4 with various damages in skin and ribs.

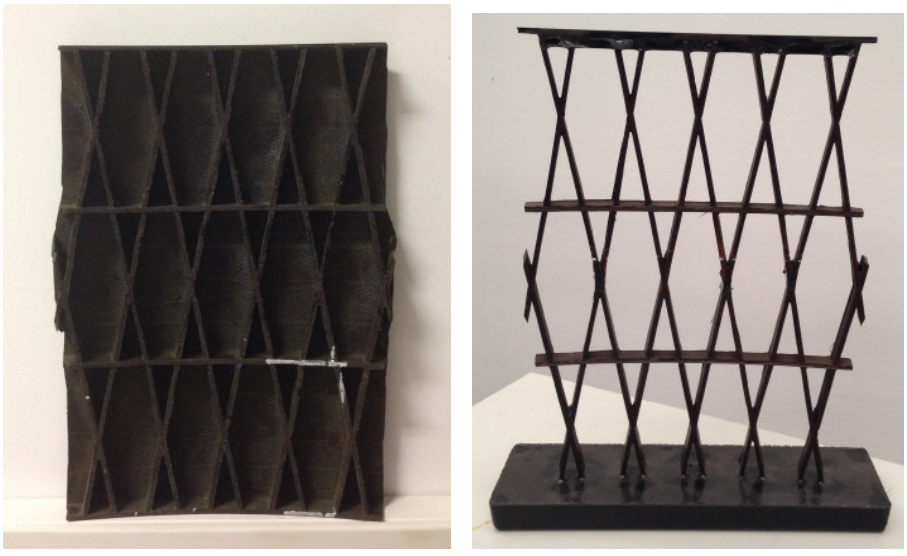

Figure 1. Anisogrid test-articles, with and without the outer skin, respectively.

Excerpt from ISBN 978-3-00-053387-7

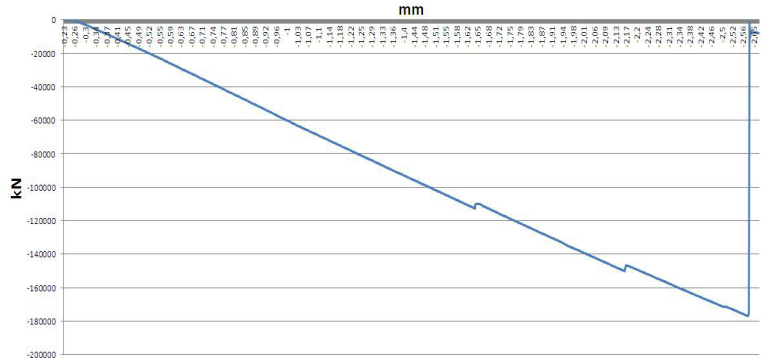

Figure 2. Load-displacement curve.

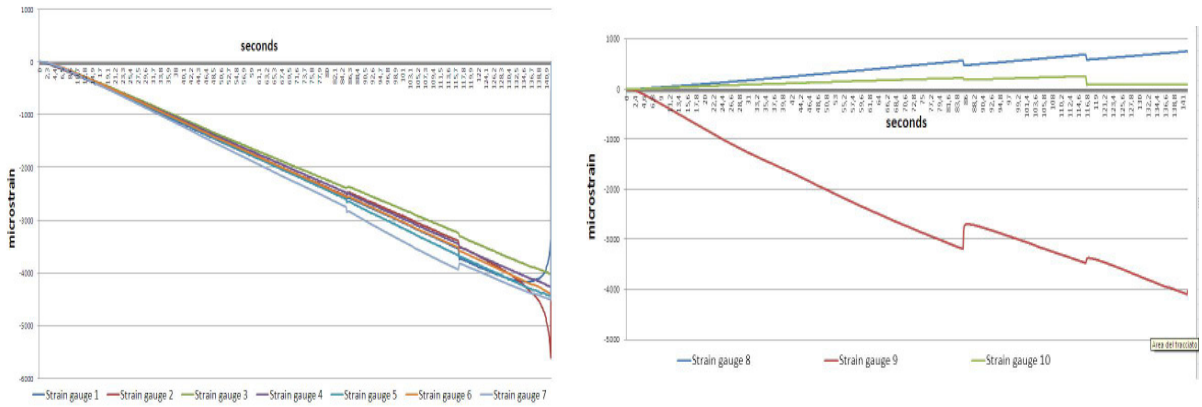

Figure 3. Strain-gauges curves on helical ribs (1-7), hoop rib (8), and skin (9-10).

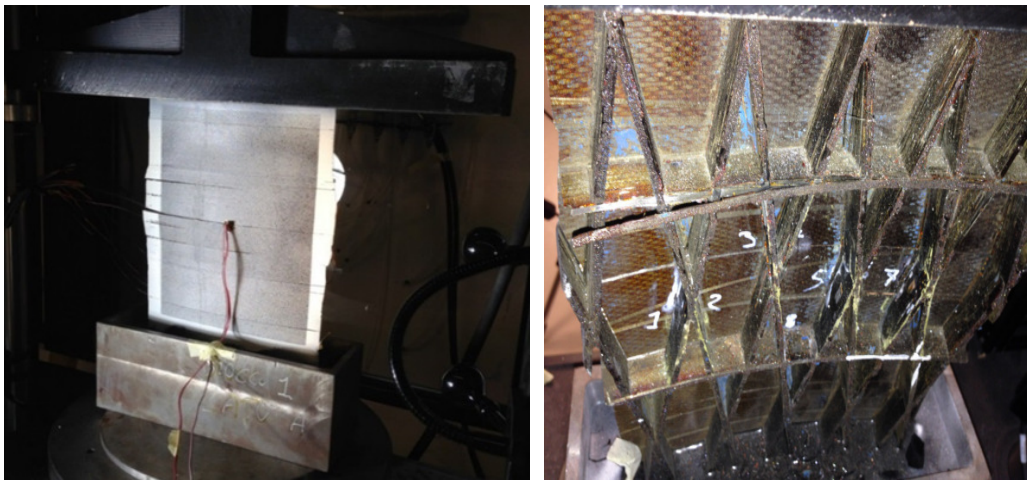

Figure 4. Anisogrid test-article after rupture.

2.1. FE model

Starting from a CAD model, a 3D FE model of the anisogrid panel was constructed in order to predict the stress field and stiffness. A reference axial compression load equal to 100 kN was applied to the master node of the rigid element placed on the top of the FE model. Examples of simulation results by

Excerpt from ISBN 978-3-00-053387-7

the Nastran solver (Figs. 5-7) show the axial shortening of the panel equal to 0.88 mm, the maximum displacement equal to 1.2 mm and 0.97 mm in hoop (transverse) and radial direction, respectively. Maximum displacements are located in correspondence of the lateral edges of the panel, where discontinuities due to the cuts clearly determine a loss of stiffness. These parts, actually, are of minor interest because are not fully representative of the behaviour of the intact continuous structure.

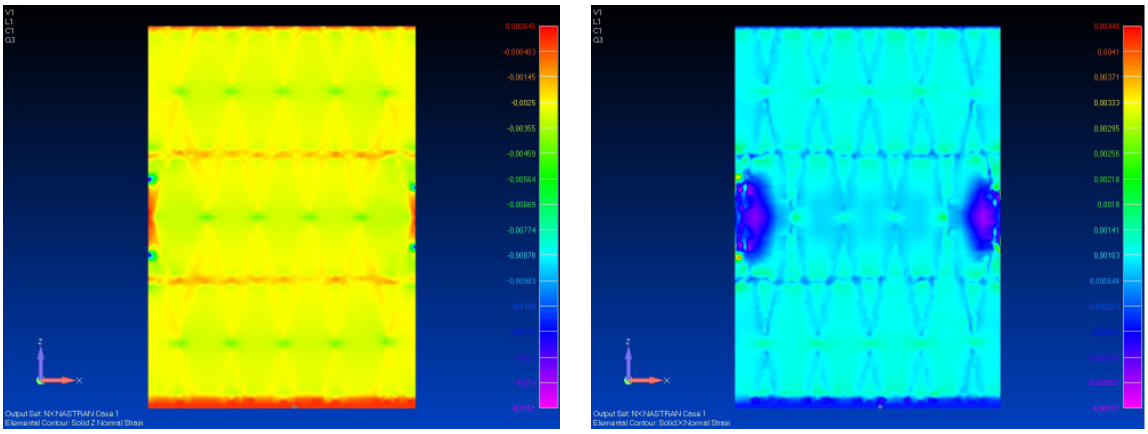

Figure 5. Axial and hoop strain, skin side of the model.

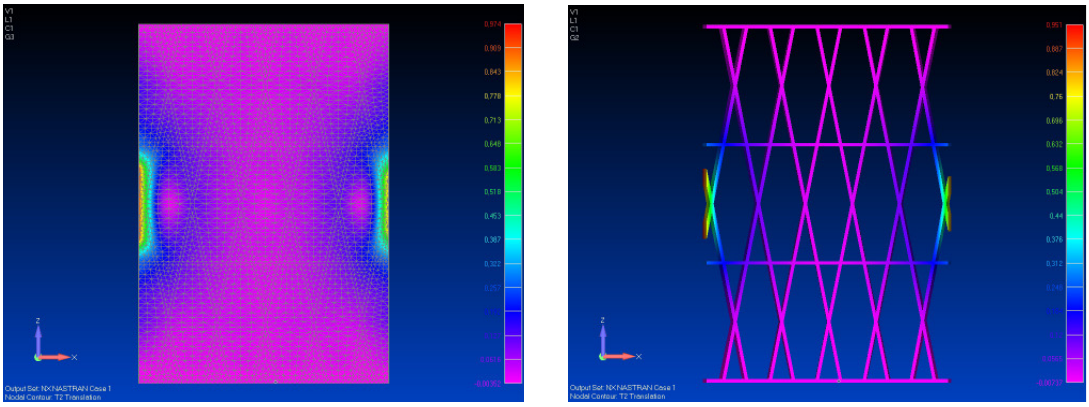

Figure 6. Radial displacement, skin and rib side.

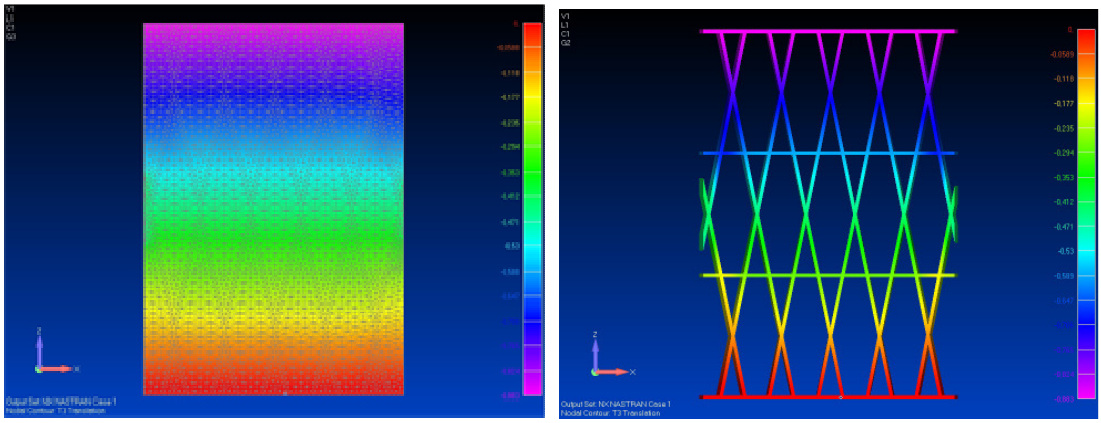

Figure 7. Axial shortening, skin and rib side.

Excerpt from ISBN 978-3-00-053387-7

2.2. Digital Image Correlation

Digital Image Correlation allows us to obtain information on displacement and deformation field by means of a stereo-camera system that provides images of the test-article during the test. The surface of the test-article to be monitored is firstly covered by a coat of white paint and then sprayed with black paint with the aid of an airbrush. The random speckle pattern is distributed over the surface and converted into a pattern of pixels. Such pixels are detected by the cameras during the displacements. The acquired images are then combined and converted into local displacements and deformations. The stereo system, in particular, allows us to detect out-of-plane (radial) displacements other than in-plane deformations. The system has been set up paying attention to the proper orientation of cameras with respect to the article and the lights surrounding the panel. The calibration phase was conducted using the calibration target with 14 mm of distance between spots, selected with respect to dimensions of the article. About 20 images were taken for each camera moving the target just ahead of the article with various angles. For the single acquisition to be valid, it is necessary that specific spots included in the calibration target are recognised by the software.

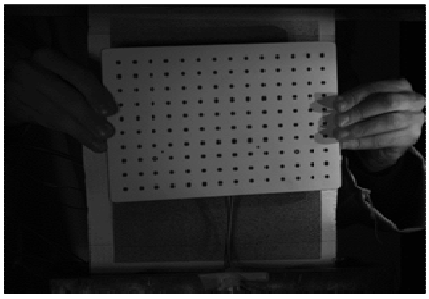

Figure 8. An image of the calibration phase (calibration target).

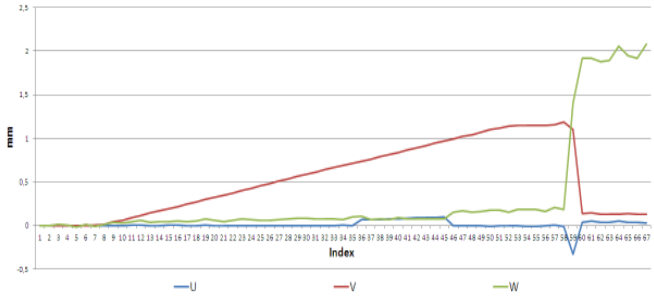

Figure 9. Axial, radial and hoop displacements (red, green, and blue line, respectively).

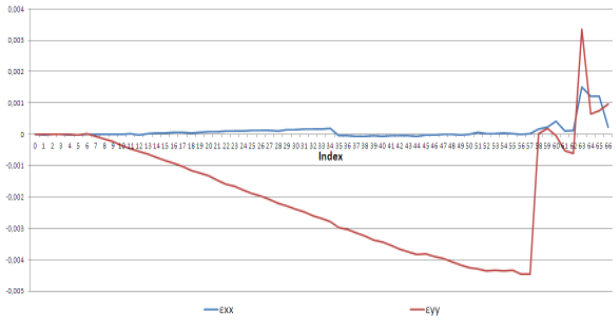

Figure 10. Axial strain (red line) and hoop strain (blue line).

Excerpt from ISBN 978-3-00-053387-7

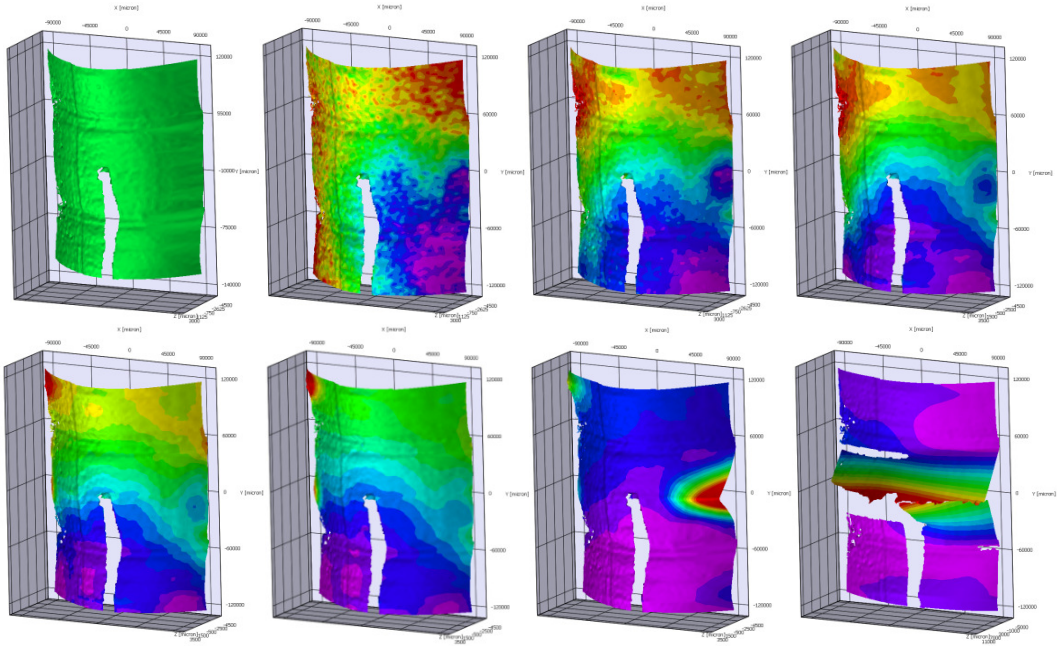

Figure 11. Radial displacement contour overlapped to total translation by DIC.

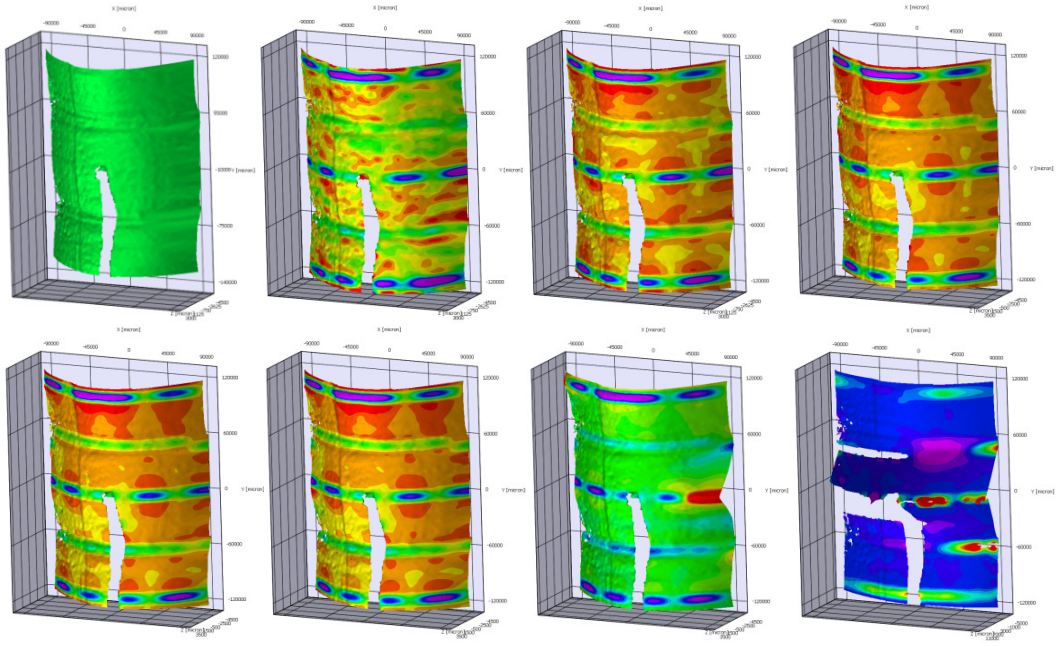

Figure 12. Axial strain contour overlapped to total translation by DIC.

Acquired images suggest a behaviour of the mechanical test much more complicated than highlighted from the FE analysis and help to understand the origin of the local failures and discontinuities. For example, while the upper part of the panel tends to move in the outward radial direction, the lower part moves in the opposite direction. This fact is visible in Fig. 11, where the blue colour represents positive radial displacement, whereas the lower part in violet represents negative displacement. This

Excerpt from ISBN 978-3-00-053387-7

effect can be probably attributed to an incorrect alignment of the panel with respect to the load axis of the testing machine, which in turn causes an irregular distribution of forces, or to pre-existing defects in the test-article (the panel is part of a structure which was previously tested under combined loads).
However, from images N°4 and N°5 of Figs. 11-12, the skin in the left upper corner seems to be highly stressed. The skin seems to move with respect to surrounding zones, causing its debonding from ribs in correspondence of 111 kN. This fact is associated with the first discontinuity that is visible in the load-displacement and strain-gauges curves (images N°4 and N°5 are taken just before and after this failure, respectively). The same effect but less pronounced, can be referred to the axial strain between the green strip (corresponding to the position of hoop ribs) and violet zones which are associated to the intersection of helical ribs (Fig. 12).
After this minor failure, images N°7 of Figs. 11-12 are referred to a significant event that precedes the structural collapse. In fact, at about 147 kN, the skin on the right side of the central section of the panel appears completely detached from the ribs. In addition, this part is the same where the two helical ribs will experience lateral buckling at around 160 kN (Fig. 3, on the left). This means that the constraint exerted by the skin on the ribs has significantly postponed this failure mode that, instead, would occur at around 100 kN involving the overall panel.

Another interesting aspect concerning the use of DIC is referred to the global axial stiffness of the panel: in fact, there is a significant difference in terms of axial displacement between the FE simulation and the evaluation based on the cross-head displacement. According to the simulation, the axial shortening in correspondence of the reference axial load (100 kN) is 0.88 mm, whereas the corresponding cross-head displacement is 1.24 mm. This relatively large difference can be explained by means of DIC images which reveal the axial displacement of the lower edge of the panel equal to 1.13 mm and the axial displacement of the upper edge of the panel about 0.26 mm. For this reason, the axial shortening of the panel detected by DIC is practically coincident with the FE simulation result (where ideal nodal constraints are normally assumed), whereas the evaluation based on the load-displacement curve would provide an axial stiffness value 30% lower than the real value.

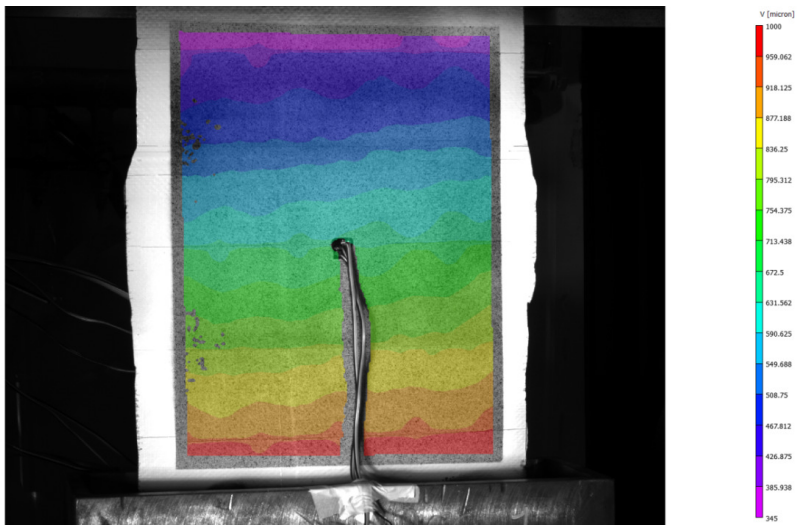

Figure 12. Axial displacement of the panel interpolated by means of DIC.

The other comparison was conducted in terms of strain-gauges data in correspondence of the reference axial load (100 kN). Simulations by FE model provide values on helical ribs included between -2850 μ and -2200 μ, whereas for the hoop rib we have about 500 μ. These values are in good agreement with strain-gauges data N° 1-8. Concerning the deformation of the skin in the central hexagonal patch, FE simulation provides the axial strain of about -3000 μ, and hoop strain about 250 μ, which fit available

Excerpt from ISBN 978-3-00-053387-7

experimental data both on the strain-gauges side (N° 9,10) and DIC side.

3. Conclusions

The effect of the skin on the strength of a composite anisogrid panel under axial compression has been preliminarily verified in this work. Starting from the maximum axial load close to 100 kN obtained in correspondence of the panel without skin - and experiencing the lateral bucking mode of ribs - the panel with skin has reached a rupture load close to 170 kN. In fact, the constraint exerted by the skin on the ribs has determined an increase of the ultimate load higher that 60%, whereas the mass increase with respect to the test-article without the skin is only 30%.
The use of the stereo-camera system with the digital image correlation software has revealed additional interesting information concerning the strain distribution and displacements, emphasizing details on the onset and position of local failures, the effect of possible misalignment of the test-article, and the presence of possible elasticity outside of the test-article. Most of these aspects would be hardly predicted a priori by the use of FE models only.

Acknowledgments

This work has been conducted within the ICCS project funded the Italian Aerospace Research Programme (PRORA).

References

[1] G. Totaro and F. De Nicola. Recent advance on design and manufacturing of composite anisogrid structures for space launchers. *Acta Astronautica,* 81:570-577, 2012. http://dx.doi.org/10.1016/j.actaastro.2012.07.012

[2] G. Totaro, F. De Nicola, and P. Caramuta. Local buckling modelling of anisogrid lattice structures with hexagonal cells: An experimental verification. *Composite Structures*, 106:734-741, 2013. http://dx.doi.org/10.1016/j.compstruct.2013.07.031

[3] G. Totaro. Local buckling modelling of isogrid and anisogrid lattice cylindrical shells with hexagonal cells. *Composite Structures*, 95:403-410, 2013. http://dx.doi.org/10.1016/j.compstruct.2012.07.011

[4] V.V. Vasiliev, V.A. Barynin and A.F. Razin. Anisogrid lattice structures – survey of development and application. *Composite Structures*, 54:361-370, 2001.

[5] C. Ferrara. Applicazioni di strutture anisogrid per gli interstadi di lanciatori spaziali. Master's Degree Thesis, Sapienza University, Rome, 2016.

Excerpt from ISBN 978-3-00-053387-7